SCIENCE CHINA
Earth Sciences

• RESEARCH PAPER •

November 2011 Vol.54 No.11: 1716–1729
doi: 10.1007/s11430-011-4290-2

Characteristics of strong earthquake evolution around the eastern boundary faults of the Sichuan-Yunnan rhombic block

CHENG Jia[1,2*], LIU Jie[1], GAN WeiJun[2], YU HuaiZhong[1] & LI Gang[1]

[1] *China Earthquake Network Center, Beijing 100045, China;*
[2] *State Key Laboratory of Earthquake Dynamics, Institute of Geology, China Earthquake Administration, Beijing 100029, China*

Received March 16, 2010; accepted April 18, 2011; published online September 27, 2011

Based on the existing materials of fault segmentation, characteristic earthquakes, and their empirical relationships, we calculated the parameters of the fault segments, such as length, width, magnitudes of characteristic earthquakes, etc. Constrained by GPS velocity field, the slip rates of these fault segments in depth were inversed using the 3-D half-space elastic dislocation model. As not all of the recurrence periods and co-seismic displacements of characteristic earthquakes are known, we selected the fault segments with these two parameters known and calculated the accumulation rate of average co-seismic displacement, which shows the faults' slip rate in seismogenic layer. Then, the slip rate in depth was compared with that in seismogenic layer, the relationship between them was obtained, and this relationship was used to get the recurrence periods and co-seismic displacements of all fault segments. After the studies above, we calculated the co-seismic deformation field of all the earthquakes larger than M_s6.8 from AD 1700 one by one and inversed the potential displacement in the co-seismic deformation field. Then, we divided the potential displacement by the slip rate from GPS inversion to get the influences of these fault segments, added the influences into the elapsed time of the characteristic earthquakes, and obtained the earthquake hazard degree of all the segments we studied in the form of the ratio of elapsed time to recurrence period; so, we name the ratio as the Impending Earthquake Risk (IER). Historical earthquake cases show that the fault segment is in safety when the IER is less than 1 but in danger after the IER becomes larger than 1. In 2009, the IER is larger than 1 on the following segments, 1.35 on the Tagong segment of Xianshuihe fault, 1 on the Menggu-Dongchuan segment, 1.04 on the Dongchuan-Xundian segment, and 1.09 on the Yiliang-Chengjiang segment of Xiaojiang fault.

eastern boundary faults of Sichuan-Yunnan rhombic block, fault segment, characteristic earthquake, recurrence period, earthquake Interaction, Impending Earthquake Risk

Citation: Cheng J, Liu J, Gan W J, et al. Characteristics of strong earthquake evolution around the eastern boundary faults of the Sichuan-Yunnan rhombic block. Sci China Earth Sci, 2011, 54: 1716–1729, doi: 10.1007/s11430-011-4290-2

The Sichuan-Yunnan rhombic block is located in the southeastern frontier of the Tibetan Plateau, and becomes the most active tectonic region after the eastward extrusion of the central Tibetan Plateau. This extrusion makes the eastern boundary faults of the Sichuan-Yunnan rhombic block have a high left-lateral slip rate with frequent strong earthquakes [1–4]. The eastern boundary faults of the Sichuan-Yunnan rhombic block consist of the Garze-Yushu fault, the Xianshuihe fault, the Anninghe fault, the Zemuhe fault, and the Xiaojiang fault [5–7].

Because of the high left-lateral slip rates and rapid energy accumulation, these faults release energy frequently through strong earthquakes. At least 18 earthquakes larger than M_s7.0 have occurred since AD 1327, including 3 larger than M_s8.0 [8]. Besides, the nearby Litang fault is also with a high frequency of strong earthquakes, of which three larger than M_s7.0 occurred on three adjacent segments in 1886,

*Corresponding author (email: chengjiajc@gmail.com)

1890, and 1948 [9]. These earthquakes may be related to the interactions among fault segments. The Daliangshan fault, which is parallel to the Anninghe fault and the Zemuhe fault, has no historical earthquake records. But recent studies proved its high left-lateral motion with frequent paleo-earthquake activities. The Daliangshan fault may have replaced the role of the Anninghe fault and Zemuhe fault in crustal deformation adjustment. This adjustment makes the Daliangshan fault a dangerous one with earthquake risks [6, 10, 11]. In order to analyze the earthquake hazard risk, it is necessary to know the following factors, the fault segmentation, the historical events on the segments, the recurrence period of characteristic earthquakes (hereafter called CERP), and the interaction among fault segments.

Fortunately, there are many studies focused on the characteristic earthquakes on the east boundary faults of the Sichuan-Yunnan rhombic block. Wen [8] described the surface rupture parameters of almost all the earthquakes larger than M_s6.5 since AD 1327, including the magnitude, rupture length, and occurrence time. Moreover, there are many other similar results on these faults [3, 12, 13].

Because of the high frequency of earthquakes on these faults, many studies have been done on the interaction among these earthquakes, and almost all the results are from the Coulomb stress changes [14–16]. Owing to the lack of the historical earthquake records and paleo-earthquake studies, it is impossible to know the recurrence period of strong earthquakes on all of these fault segments. So, no comprehensive studies have been done on the CERP, earthquakes interactions, and earthquake hazard analysis.

Here we carry out a comprehensive study in the following steps.

(1) We will divide the eastern boundary fault zone into detailed characteristic earthquake segments, and analyze the empirical relationships among the rupture parameters to get more reasonable results, including the rupture length, width, average co-seismic displacement, and so on.

(2) We will collect and sort the material of paleo-earthquakes and detailed historical earthquake records of some fault segments that have more research results, determine the recurrence period of strong earthquakes on these fault segments, and obtain the average slip rate from the ratio between the average co-seismic displacement and recurrence period.

The average slip rate we obtained represents the accumulation rate of co-seismic displacement (hereafter we call the slip rate V_{eq}) in the seismogenic layer, showing the energy accumulation rate of earthquakes.

(3) We will inverse the slip rate of all the fault segments in depth (hereafter we call the rate V_{gps}) in the crustal deformation field constrained by GPS data, and obtain the relationship between V_{eq} and V_{gps}.

(4) According to the relationship above and V_{gps} of all the fault segments, we can get V_{eq} of all the segments, and determine the recurrence period of characteristic earthquakes (CERP), which is the ratio between the average co-seismic displacement and V_{eq}. Then we can get the elapse degree of characteristic earthquakes through dividing the elapsed time by the recurrence period, calculate the co-seismic deformation field of all the earthquakes larger than M_s6.8 since 1700 using the parameters obtained above, inverse all V_{gps}, and give the influence degree of these earthquakes by the ratio between influence value and V_{gps}.

Eventually we can get the Impending Earthquake Risk degree after adding the elapse degree and influence degree, and determine the earthquake risk of fault segments using the Impending Earthquake Risk.

1 Distribution of strong earthquakes and division of fault segments

1.1 Fault segmentation around the eastern boundary fault zone of Sichuan-Yunnan rhombic block

The eastern boundary fault zone is composed of a number of faults, namely, the Garze-Yushu, Xianshuihe, Anninghe, Daliangshan, Xiaojiang, and Litang faults. Meanwhile, almost all the segments of the fault zone have surface rupture tracks. Reasonable fault segmentation is crucial for the study of characteristic earthquakes interaction and earthquake hazard risks [17]. In this paper, we will give a more refined segmentation model of the faults after analyzing the data of earthquake rupture parameters and previous segmentation model (Figure 1).

The segmentation of Xianshuihe fault is based on the model of Wen [18]. As to the overlapping section of fault branches, we have divided it into two parts at the mid-point and attached each part to its main side. However, for the earthquakes with $M7^3/_4$ in 1786 and $M7^1/_2$ in 1955, the overlapping section has been assumed as a single segment, given that the rupture zone of the earthquake in AD 1786 may be a cascade rupture event of the Moxi segment and the overlapping section. Also at the section between Qianning and Kangding, the Xianshuihe fault has three sub-parallel faults, namely, the Yalahe sub-fault, the Selaha-Kangding sub-fault, and the Zheduotang sub-fault; we have divided this fault section into two segments, 31 and 44 km in length respectively, according to the surface rupture distribution of the Kangding earthquake in 1955.

As to the Zemuhe fault, Li [3] pointed out that the dip direction of the fault may have changed in the Qionghai basin. Zhang and Ren [19] also suggested that the fault should be divided into two segments at the same place, based on the view that the character of motion is stick-slip in the north segment but creep in the south. Thus, we thought that the Zemuhe fault should be composed of two fault segments, with the separation point in the Qionghai basin. The $M6^3/_4$ earthquake in 1732 occurred on the north segment of Zemuhe fault whereas the earthquake in 1850

ruptured the whole fault. The magnitude of the earthquake in 1850 is still in debate [12, 20, 21]. Wen et al. [21] held that the earthquake has ruptured the whole fault after having analyzed the characters of the surface rupture, and indicated that the magnitude should be larger than $M7^1/_2$. Ren [12] argued that the co-seismic displacement of the earthquake in 1850 should be equivalent to that of an *M*8 earthquake. In addition, Li [3] reported that the recurrence period of *M*8.0 earthquakes on the Zemuhe fault was 885–1275 based on the studies of paleo-earthquake in Holocene.

Similarly, the segmentation of other faults is based on the results of previous studies. The segmentations of these faults are shown in Figures 1, 2 and Table 1, including the Garze-Yushu fault [22], the Anninghe fault [23], the Xiaojiang fault [2, 8], the Daliangshan fault [10] and the Litang fault [9]. This segmentation model and the strong earthquakes occurring on the fault segments can help us study the interaction among earthquakes and earthquake hazard risk.

1.2 Parameters of earthquake rupture segments and their self-adaptive relationships

Although studies are focused on these faults, especially on the size of earthquake ruptures, detailed descriptions on the other parameters, such as the rupture width, co-seismic displacement, etc., are seldom seen. Many relationships exist among the magnitude of the earthquakes and these parameters [29–31], and the most well-known is that of Wells [31], which is based on the statistical studies of the global earthquake rupture data. Given that the movement of these faults is mainly left-lateral strike-slip, the dip-slip component is ignored in this paper, with the GZIF as an exception. Thus, we selected the formulas of Wells [31] as shown by eqs. (1)–(5):

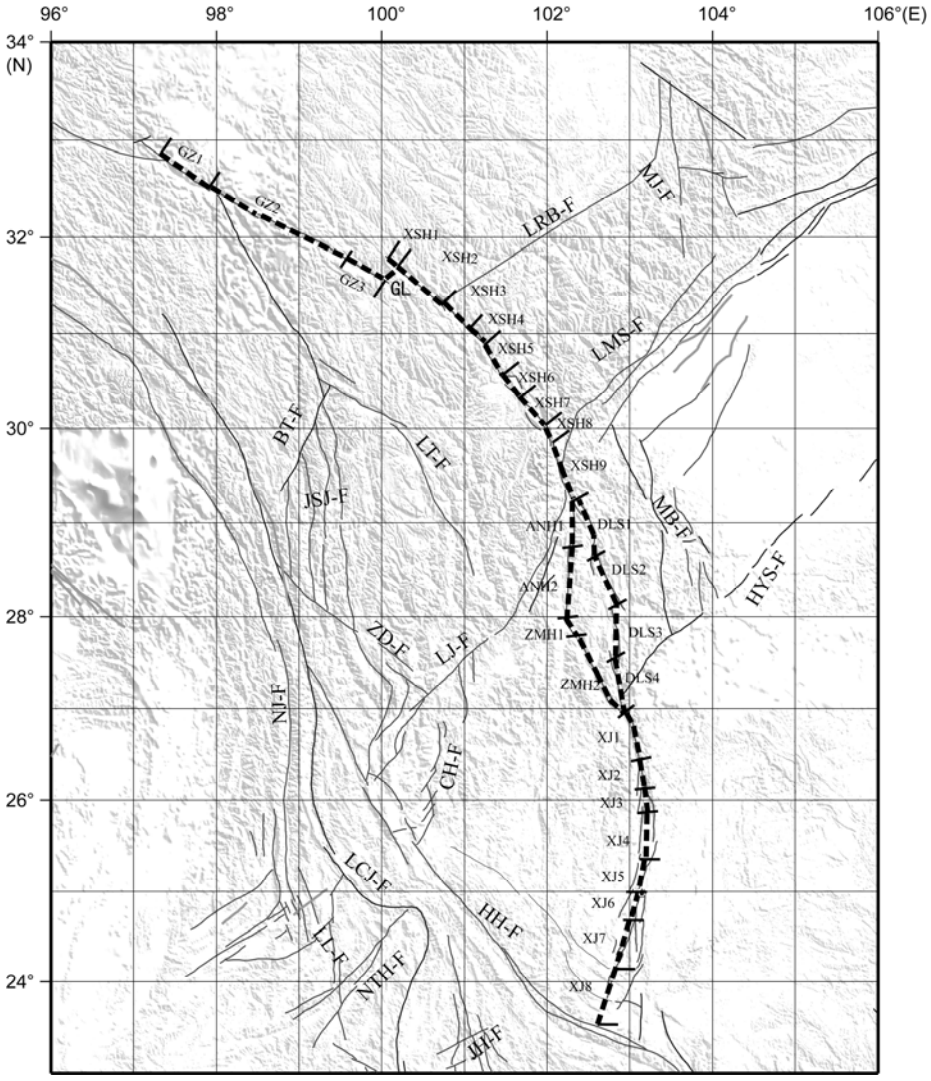

Figure 1 Distribution of faults in Sichuan-Yunnan region and segmentation of the east boundary faults of Sichuan-Yunnan rhombic block. GZ, Garze-Yushu fault; GL, GZIF, Garze inner fault; XSH, Xianshuihe fault; ANH, Anninghe fault; ZMH, Zemuhe fault; DLS, Daliangshan fault; XJ-F, Xiaojiang fault; LT-F, Litang fault; LRB-F, Longriba fault; LMS-F, Longmenshan fault; MJ-F, Minjiang fault; LJ-F, Lijiang-Xiaojinhe fault; CH-F, Chenghai fault; BT-F, Batang fault; JSJ-F, Jinshajiang fault; ZD-F, Zhongdian fault; HH-F, Honghe fault; LCJ-F, Langcangjiang fault; NJ-F, Nujiang fault; NTH-F, Nantinghe fault; LL-F, Longling-Langcangjiang fault; JH-F, Jinghong fault; MB-F, Mabian fault; HYS-F, Huayingshan fault.

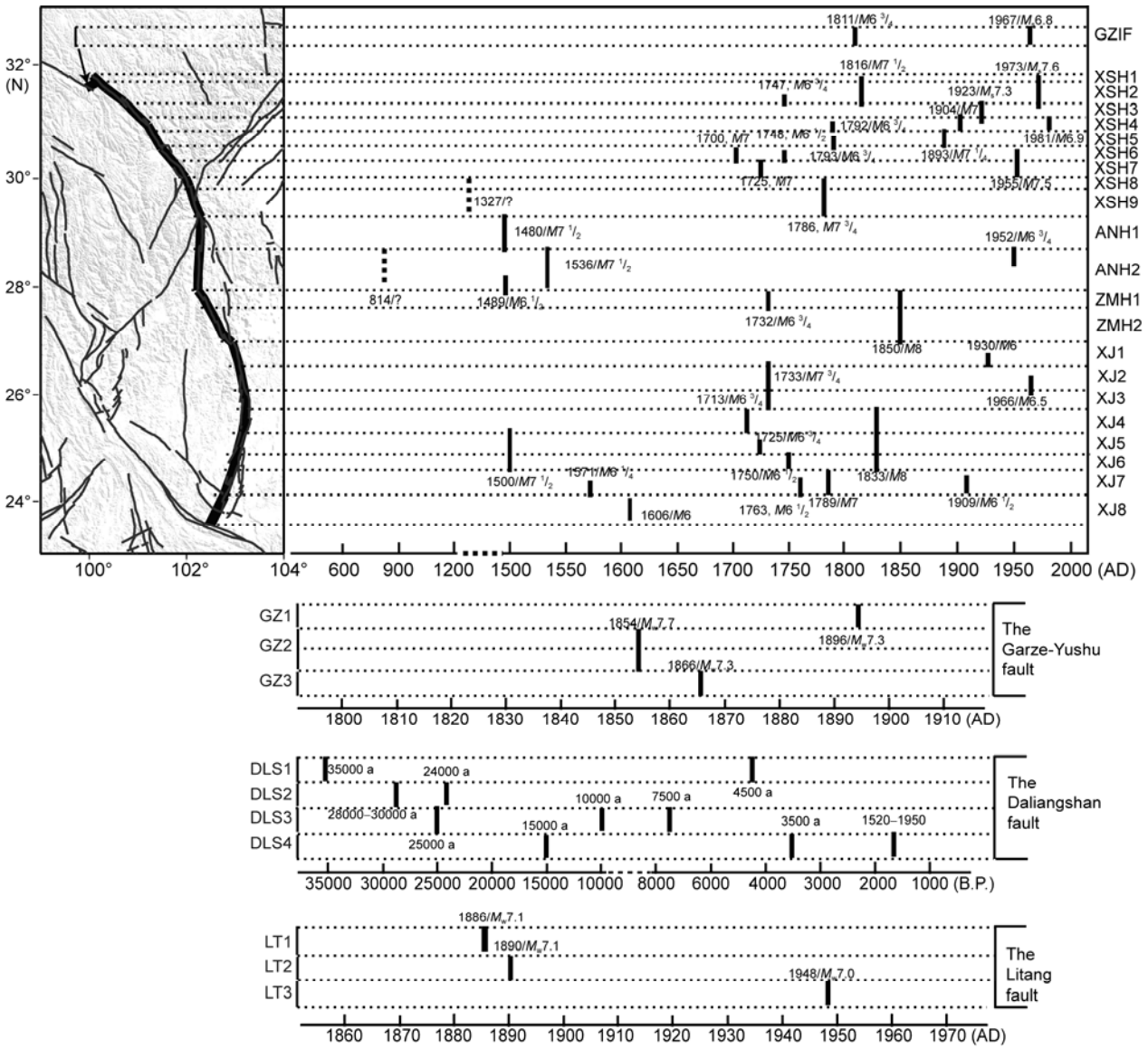

Figure 2 Segmentation of the east boundary faults and historical earthquakes.

$$\log(\mathrm{SRL}) = -3.55 + 0.74 \times M, \tag{1}$$

$$\log(\mathrm{RW}) = -0.76 + 0.27 \times M, \tag{2}$$

$$\log(\mathrm{RA}) = -3.42 + 0.90 \times M, \tag{3}$$

$$\log(\mathrm{AD}) = -6.32 + 0.90 \times M, \tag{4}$$

$$M = 6.81 + 0.78 \times \log(\mathrm{MD}), \tag{5}$$

where M is the moment magnitude, SRL the surface rupture length, RW the rupture width, RA the rupture area, MD the maximum co-seismic displacement, and AD the average co-seismic displacement.

For the conversion among M_w, M_s, and M_0, we have used eq. (6); it was given for strike-slip faults based on all the earthquakes larger than M_s5.0 during 1977 to 2001 in China [32]. Eq. (7) expresses the relation between M_w and M_0, with M_0 measured in N·m:

$$\log M_0 = 1.64 \cdot M_s + 7.56, \tag{6}$$

$$M_w = \frac{2}{3}\log M_0 - 6.033. \tag{7}$$

In view of the specialty of the regional tectonic environment, the applicability of the relationships should be checked. To compare the parameters observed from fieldwork with those calculated from Wells' formulas, we have done some tests on the fault segments with enough parameters. Table 2 and Figure 3 show the results.

As to the rupture length, the results are in good agreement with each other in most cases, but the Qianning earthquake in 1893 is an exception. We considered that the rea-

Table 1 Fault segmentation and rupture parameters of the east boundary fault zone of Sichuan-Yunnan rhombic block

Fault zone name	Segment interval	Segment ID	Length (km)	Geological slip rate		Characteristic earthquakes	Maximum horizontal co-seismic displacement (m)	Average recurrence period (a)	Observed recurrence period (a)	Reference
				Strike-slip (mm/a)	Thrust (mm/a)					
Garze-Yushu	Batang-Luoxu	GZ1	70	12±2	–0.6– –1.2	M_w7.3 in 1896	5	–	–	[22, 24]
	Luoxu-Yakou	GZ2	180			M_w7.7 in 1854	9	–	–	
	Yakou-Tingka	GZ3	65			M_w7.3 in 1866	5.3	–	–	
GZIF	Tingka-Zhuwo	GL	20	–	–	$M6^3/_4$ in 1811 M6.8 in 1967	–	–	156	[16]
Xianshuihe fault	Donggu-Zhuwo	XSH1	20			M7.6 in 1973				[25]
	Luohuo	XSH2	70	8.8±3.5		$M7^1/_2$ in 1816 M7.6 in 1973	4	131–161	157	[4, 18, 25–27]
	Renda	XSH3	45	10–15	–	M_s7.3 in 1923	3	93–126	–	
	Daofu	XSH4	33	10–15	–	M7 in 1904 M_s6.9 in 1981	0.78	70–96	77	
	Qianning	XSH5	54	10–15	–	$M \geqslant 7^1/_4$ in 1893	2.44	84–118	100–101	
	Tagong	XSH6	31	7.5±0.8	–	–	–	197–269	–	
	Kangding	XSH7	44	9.1±0.9	–	M7 in 1725 $M7^1/_2$ in 1955	3	225–310	230	
	Kangding-Xindianzi	XSH8	20	9.9±0.6	–	$M7^3/_4$ in 1786 $M7^1/_2$ in 1955	–	–	169	
	Moxi	XSH9	90	9.9±0.6	–	$M7^3/_4$ in 1327 $M7^3/_4$ in 1786	–	360–490	459	
Anninghe fault	North of Mianning	ANH1	62	3.8±4.2	1.4	$M7^1/_2$ in 1480	3±0.5	520–660	–	[13]
	South of Mianning	ANH2	84	5–8	–	$M7^1/_2$ in 814 $M7^1/_2$ in 1536	–	–	722	
Zemuhe fault	North segment	ZMH1	23	6.4±0.6	–	$M6^3/_4$ in 1732 ~M8 in 1850	–	885–1275	118	[19]
	South segment	ZMH2	108	6.4±0.6	–	~M8 in 1850	–		1226	[3]
Xiaojiang fault	Qiaojia-Menggu	XJ1	50	10±2	–0.2– –0.7	–	–	–	–	[10]
	Menggu-Dongchuan	XJ2	45	10±2	–0.2– –0.7	$M7^3/_4$ in 1733	–	~1000	~900	[2, 3, 28]
	Dongchuan-Xundian	XJ3	40	10±2	–0.2– –0.7	$M7^3/_4$ in 1733	–			
	Xundian-Songming	XJ4	48	10±2	–0.2– –0.7	M8 in 1833	–	830–930	–	[2, 3, 10]
	Songming-Yiliang	XJ5	48	10±2	–0.2– –0.7	$M7^1/_2$ in 1500 M8 in 1833	–		333	
	Yiliang-Chengjiang	XJ6	32	10±2	–0.2– –0.7	$M7^1/_2$ in 1500 M8 in 1833	–		333	
	Chengjiang-Tonghai	XJ7	60	10±2	–0.2– –0.7	–	–	–	–	[8]
	Tonghai-Jiangshui	XJ8	60	–	–	–	–	–	–	
Daliangshan fault	Shimian-Yuexi	DLS1	73	1–3	–	35000 a B.P. 4500 a B.P.	–	–	–	[10, 11]
	Puxiong-Zhuhe	DLS2	66	2	–	28000–30000 a B.P. 24000 a B.P.	–	–	–	
	Tuodu-Butuo	DLS3	62	2.6–3.9	–	25000 a B.P. 10000 a B.P. 7500 a B.P.	–	–	–	
	Jifulada-Jiaojihe	DLS4	65	3	–	15000 a B.P. 3500 a B.P. 1520–1950 a B.P.	–	–	–	
Litang fault	Maoyaba	LT1	55	4	0.1–1.8	M_w7.1 in 1886	4.1	–	–	[9]
	Litang	LT2	50	4	0.1–1.8	M_w7.1 in 1890	⩾4	500–1000	–	
	Kangga-Dewu	LT3	40	4	0.1–1.8	M_w7.0 in 1948	4.3	–	–	

Table 2 Characteristic earthquakes on fault segments and related rupture parameters

Fault segment ID	M_s of characteristic earthquake	Rupture size: Length (km)		Rupture size: Width (km)		Maximum co-seismic displacement (m)		Average co-seismic displacement (m)		Recurrence period (a)		Time (AD, year)		V_{eq} (mm/a)		V_{gps} (mm/a)	
		This paper	Wells	This paper	Wells	Observed	Wells	Wells	This paper	Historical records	This paper		From historical earthquake studies	This paper	Strike slip	Dip slip
GZ1 [22]	7.6	70	71	15	16.3	5	4.2	2.5	3.35	–	356±24	1896	–	9.4±0.8	12.0±0.8	–0.1±0.9
GZ2 [22]	8.0	180	141	15	21	9	13.8	6.1	4.91	–	517±34	1854	–	9.5±0.8	12.1±0.8	–0.5±0.9
GZ3 [22]	7.6	65	71	15	16.3	5.3	4.2	2.5	3.61	–	391±41	1866	–	9.5±1.0	12.1±1.0	–0.2±0.9
GL [16]	6.8	20	–	15	–	–	–	–	0.23	156	256±110	1811–1967	–	1.1±0.6	1.4±0.6	–4.1±0.9
XSH1	6.8	20	73	15	16.4	4	4.5	1.84	0.57	–	⩾403	–	–	0.24±1.5	0.3±1.5	0.0±0.9
XSH2 [16]	7.5	70							2.3	157	240±26	1816 1973	16.7	9.7±1.3	12.3±1.3	–0.1±0.8
XSH3 [16]	7.3	45	42	15	13.4	3	1.7	0.9	1.7	–	176±16	1923	–	9.6±1.5	12.2±1.1	–0.1±0.8
XSH4 [16]	7.0	33	24	15	10.9	0.78	0.64	0.47	0.74	77	78±7	1904 1981	9.6	9.5±1.1	12.1±0.7	–0.1±0.8
XSH5 [16]	7.3	54	38	15	12.9	2.44	1.44	1.2	1.4	–	144±13	1893	–	9.8±1.4	12.4±0.7	–0.1±0.8
XSH6 [16]	7.1	31	–	15	–	–	–	–	1.7	–	192±20	–	–	8.8±1.2	11.2±0.7	–0.1±0.8
XSH7 [16]	7.3	44	61	15	15.3	3	3.2	1.5	1.7	230 –	193±19	1725 1955	10.9 –	8.9±1.1	11.4±0.9	0.5±0.6
XSH8 [16]	6.8	20							0.84	459	95±9	1786	8.3	8.9±1.0	11.3±0.9	0.6±0.6
XSH9	7.5	70	–	15	–	–	–	–	2.3	–	285±39	1327	–	8.2±1.4	10.4±0.9	1.2±0.6
ANH1 [8]	7.5	62	61	15	15.3	3±0.5	3.2	1.5	2.6	520-660	518±72	1480	4.4±0.6	5.1±0.9	6.5±0.9	0.6±0.6
ANH2	7.7	84	–	15	–	–	–	–	4.1	722	708±77	814 1536	–	5.8±0.8	7.4±0.8	0.6±0.6
ZMH1	6.9	23	–	15	–	–	–	–	0.73	118 1226	149±17	1732 1850	–	5.0±0.7	6.3±0.7	–1.3±0.6
ZMH2	7.8	108	–	15	–	–	–	–	4.6	–	850±98	–	–	5.5±0.8	7.0±0.8	–1.3±0.6
XJ1	7.4	50	–	15	–	–	–	–	2.2	–	282±26	–	–	7.9±0.9	10.0±0.9	–0.7±0.6
XJ2	7.3	45	–	15	–	–	–	–	1.7	900	220±25	1733	–	7.7±1.1	9.8±1.1	–0.7±0.6
XJ3	7.3	40	–	15	–	–	–	–	1.9		249±23		–	7.6±0.9	9.7±0.9	–0.7±0.6
XJ4	7.3	48	–	15	–	–	–	–	1.6	–	200±22	–	–	8.0±1.1	10.1±1.1	–0.7±0.6
XJ5	7.3	48	–	15	–	–	–	–	1.6	333	200±22	1500 1833	–	8.0±1.1	10.1±1.1	–0.7±0.6
XJ6	7.1	32	–	15	–	–	–	–	1.1		143±13		–	7.8±0.9	9.9±0.9	–0.7±0.6
XJ7	7.5	60	–	15	–	–	–	–	2.7	–	365±35	–	–	7.4±0.9	9.4±0.9	–0.7±0.6
XJ8	7.5	60	–	15	–	–	–	–	2.7	–	508±48	–	–	5.0±1.1	6.3±1.1	–0.7±0.6
DLS1	7.6	73	–	15	–	–	–	–	3.2	–	1065±213	–	–	3.1±0.8	4.0±0.8	0.5±0.6
DLS2	7.5	66	–	15	–	–	–	–	2.4	–	806±162	–	–	3.1±0.8	4.0±0.8	0.5±0.6
DLS3	7.5	62	–	15	–	–	–	–	2.6	–	860±172	–	–	3.1±0.8	4.0±0.8	0.7±0.6
DLS4	7.5	65	–	15	–	–	–	–	2.5	–	820±164	–	–	3.1±0.8	4.0±0.8	0.5±0.6
LT1 [9]	7.4	55	–	15	–	–	–	–	2.0	–	620±130	1886	–	3.4±0.9	4.3±0.9	0.5±0.6
LT2 [9]	7.4	50	51	15	14.4	4.1	2.4	1.2	2.2	–	649±130	1890	–	3.4±0.9	4.5±0.9	0.5±0.6
LT3 [9]	7.3	40	43	15	13.5	4.3	1.8	1	1.9	–	555±111	1948	–	3.4±0.9	4.5±0.9	0.4±0.6

sons should be as follows. Heim [33] pointed out that the surface rupture extended from Songlinkou to Huiyuansi for about 54 km, which was also confirmed by later fieldwork [4, 34]. However, according to the empirical relationships, both the rupture length and the maximum co-seismic displacement are larger than those of an $M7^1/_4$ earthquake. Therefore, we considered that the magnitude of the earthquake should be M_s7.4, with a rupture length of 50 km and maximum co-seismic displacement of 2.34 m, as given by eqs. (1)–(5), which are consistent with the results of fieldwork.

For the rupture width of the fault segments, Wells has given the statistic relationship between magnitude and rupture width (depth), too [31]. However, it should be considered that the temperature of crust in the lithosphere increased gradually with the depth, and there is some depth where the structure of the lithosphere transits from elastic to plastic in character. The rupture of the earthquake is constrained above the depth probably, especially when the earthquake is an intraplate event; this depth can be called the locking depth, while the upper layer above the locking depth is called the seismogenic layer. Zhu et al. [35] suggested that the average locking depth of the crust is about 15 km in Sichuan-Yunnan region from the relocation of small earthquakes. Wang et al. [6] also found that the inversion residual of the GPS data becomes the minimum when

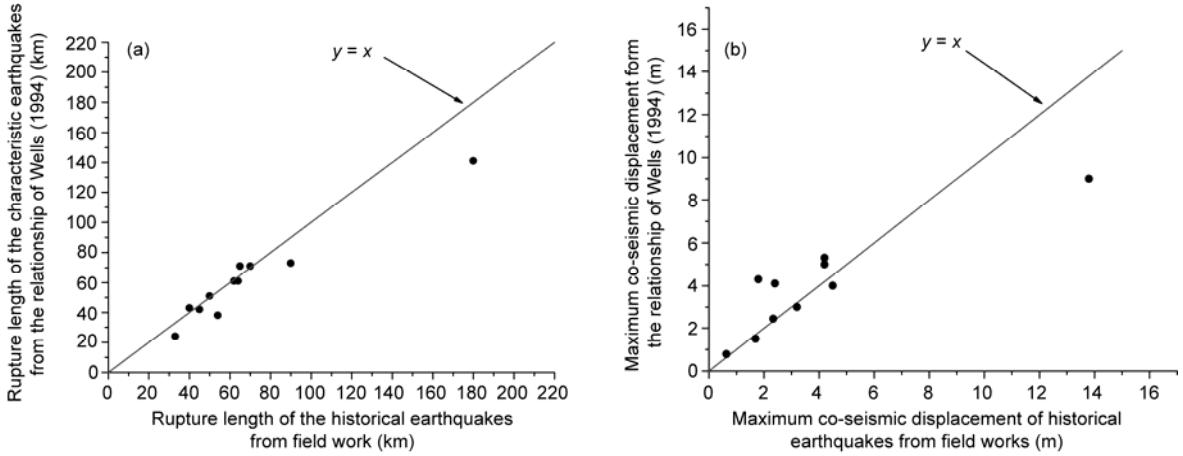

Figure 3 Comparison between the results of Wells' empirical formulas and those of field work. (a) Rupture length; (b) maximum co-seismic displacement.

the locking depth of the faults is about 15 km. because of these studies, we did not calculate the rupture width from Wells' formulas but considered 15 km as the rupture width of all the fault segments.

The maximum co-seismic displacements observed in fieldwork differ little from those calculated by Wells' formulas. The most obvious discrepancy is seen in the data of the Renda earthquake in 1923, and the magnitude and maximum co-seismic displacement are M_s7.3 and 3 m respectively from ref. [16]. The data were cited from Allen et al. [4], who described the maximum co-seismic displacement of the Renda earthquake with uncertainty, and deduced this displacement as the sum of two events. In that case, the maximum co-seismic displacement of the Renda earthquake is about 1.5 m, close to the result of Wells' formula. In Figure 3(a) and (b), the rupture length and maximum co-seismic displacement from fieldwork are compared with those from formula for each earthquake. The figures show that the larger the magnitude of earthquake is, the more the increases of rupture length and co-seismic displacement would be, especially for earthquakes greater than M_s7.5. This explains the deviation of the M_w7.7 earthquake in 1854 in Figure 3.

As to the earthquakes occurring on the Litang segment and Kangga-Dewu segment, Xu et al. [9] deduced that the magnitude of the Litang earthquake is M_w7.1 from rupture length but M_w7.3 from the maximum co-seismic displacement using Wells' formula, whereas the magnitude of the earthquake on the Kangga-Dewu segment is M_w7.0 from rupture length but M_w7.3 from the maximum co-seismic displacement.

As the maximum co-seismic displacement is likely to be affected by irregular rupture and local structures, the rupture length always has some errors. So we used the formula between the magnitude and rupture length, eq. (1), to get the magnitude of the two earthquakes. Thus, the magnitude of earthquake on the Litang segment is M_w7.1, and the magnitude of that on the Kangga-Dewu segment is M_w7.0. This process has eventually caused the deviation between the observed and calculated results of the maximum co-seismic displacement in Figure 3(b).

The above studies reveal that the statistic formulas of Wells are applicable in this region, especially the relationship among the magnitude of earthquakes, rupture length, and the maximum co-seismic displacement. Therefore, we can use these formulas to calculate the rupture parameters from the magnitude or deduce the magnitude from rupture parameters. As to the magnitude of historic earthquake records, ¼ means 0.1~0.4, ½ means 0.4~0.6, and ¾ means 0.7–0.9 in this paper.

As the average co-seismic displacement from fieldwork is not very accurate, Wells' formula also has large errors. Thus, we have used the scalar seismic moment to calculate the average co-seismic displacement when the rupture length and width are known. The formula is as follows and the results are shown in Table 2:

$$M_0 = \mu \cdot L \cdot W \cdot D. \tag{8}$$

In eq. (8), μ is the rigidity of the elastic layer; L is the rupture length; W is the rupture width; D is the average co-seismic displacement; μ=3×10^{10} N/m^2; and W=15 km. Table 2 gives the calculation results.

1.3 Slip rate of the fault segments

In order to check the reasonableness of our calculated rupture parameters, we should obtain the present-day slip rates of the fault segments. This also can help us calculate the Recurrence Period of the Characteristic Earthquakes (CERP). Once the average co-seismic displacement and CERP become known, we can calculate V_{eq}. Meanwhile we can inverse the long-term slip rate of the fault segments in depth (V_{gps}) using GPS data. The comparison between V_{eq} and V_{gps} will reflect the feasibility of our method.

(1) Accumulation rate of co-seismic displacement (V_{eq}). The CERP that we have collected from previous studies can be divided into two parts. One is from the ratio of the aver-

age co-seismic displacement and the average accumulation rate in geological history. For example, the average CERP of the segments on Xianshuihe fault was given by Wen [26], i.e. the 888–1275 years' CERP of M_s8 earthquake on the Zemuhe fault, about 1000 years' CERP of the Dongchuan event in 1533 on Xiaojiang fault, and the 830-930 years' CERP of the Songming earthquake in 1833 of the Xiaojiang fault [3]. The other is from the average time interval of events in geological history. For example, Ran et al. [13] pointed out that the CERP of the north segment on the Anninghe fault is 520–660 years from the average time interval of three earthquakes in the last 1700 years. Li [3] thought that the CERP of the Dongchuan earthquake in 1733 is about 900 year from ^{14}C dating result of two paleo-earthquakes. In that case, if we use the data from the first method to calculate V_{eq}, we will fall into the trap of a loop calculation when using the CERP calculated from V_{eq} to calculate V_{eq}. Thus, we have only used the CERP obtained by the second method, which means the average interval of recurrence paleo-earthquakes or historical earthquakes.

The GZIF is not a main boundary fault but a fault segment of small size in the Garze pull-apart basin; and the basin lies between the Garze-Yushu fault and Xianshuihe fault. Two M_s6.8 events have occurred on the GZIF, with rupture length of 20 km, left-lateral displacement of 0.23 m and tensile displacement of 0.64 m. Considering the specialty of the GZIF, we assumed that the rupture length of the fault segment is 20 km, the strike-slip displacement is 0.23 m, the tensile displacement is 0.64 m, and the dip angle is 85°. The average displacement of the GZIF segment is D, $D=\sqrt{(0.23/\sin 85^\circ)^2+0.64^2}=0.68$ m. The rupture width can be obtained to be 12.6 km from eq. (8).

To sum up, we have obtained the average co-seismic displacement and V_{eq} of the fault segments with enough data. Table 2 shows the results.

(2) Slip rate of fault segments inversed from GPS (V_{gps}). The slip rates inversed from GPS data are only for the whole fault [6, 7], but not for the fault segments we have divided. Therefore, we inversed the slip rates in depth of the fault segments in our model using the GPS data. And the results will be compared with the accumulation rate of co-seismic displacement (V_{eq}) in seismogenic layer to see the feasibility of our method.

The 3-D half-space elastic dislocation model we used is based on the Okada's elastic dislocation theory [36–41], and has been adopted in the co-seismic deformation field calculation and the slip rates inversion widely. In the model, the crust is seen as an elastic body, and the fault is seated under the locking depth. The locking depth divides the crust into two layers, seismogenic layer in shallow place and dislocation layer in deep place. In the interseismic period, the fault can be explained as the continuous movement of dislocation while the seismogenic layer is locked. In the co-seismic period, the seismogenic layer ruptures abruptly while the dislocation layer is locked relatively. After the earthquake, the seismogenic layer will heal over for years, with the adjustment of post-seismic deformation.

The GPS data we used are from Shen et al. [7], which are obtained by 248 GPS stations in several phases of observation. The fault geometric model and parameters in this paper are cited from previous studies [42]. The fault parameters include the strike, dip direction, dip angle, and locking depth. The locking depth is 15 km in the Sichuan-Yunnan rhombic block but 20 km in the Sichuan basin. Based on the 3-D fault geometric model and fault segmentation, we inversed the slip rate in depth of these fault segments. Firstly, we inversed the slip rate of the east boundary fault zone with more GPS stations around. Then we added the results of the first step into the geometric model as initial value and inversed the slip adjustment of other faults. The inversion results are shown in Figure 4 and Table 2.

The results are similar to those of rigid block motion model [7] and linked-fault element model [6]. But our model has taken the dip angles of all the faults into consideration, which makes our results more practical.

(3) The relationship between V_{eq} and V_{gps}. Comparing V_{eq} in seismogenic layer and V_{gps} in depth on the specific segments (Table 2 and Figure 5), we will find that V_{gps} and V_{eq} have good conformity, which means that the segments with high V_{gps} are also with high V_{eq}. In order to obtain the statistic relationship between V_{eq} and V_{gps}, we first removed the two events with maximum or minimum ratio of V_{eq} and V_{gps}. Then we got the statistic proportion of them (eq. (9)):

$$V_{eq}=0.7873\times V_{gps}. \tag{9}$$

After that, we can use this formula to calculate all the V_{eq} via V_{gps}, then use the average displacement of characteristic earthquakes ($\bar{D}$) and V_{gps} to calculate the Recurrence Period of Characteristic Earthquakes (CERP). Table 2 shows the results.

2 Co-seismic deformation fields and their influence on other fault segments

With the parameters of earthquakes on the fault segments known, we can first calculate the co-seismic deformation field and then inverse the potential displacement of other fault segments in the co-seismic deformation field. This potential displacement can reflect the energy accumulation or release of the other segments during the earthquake. In order to calculate the potential displacement, we chose a time-window from AD 1700 to AD 2009, in which historical records are more complete and more than half of the studied fault segments have been hit by earthquakes.

During the calculation of the earthquakes larger than M_s6.8 since 1700, each earthquake was regarded as having

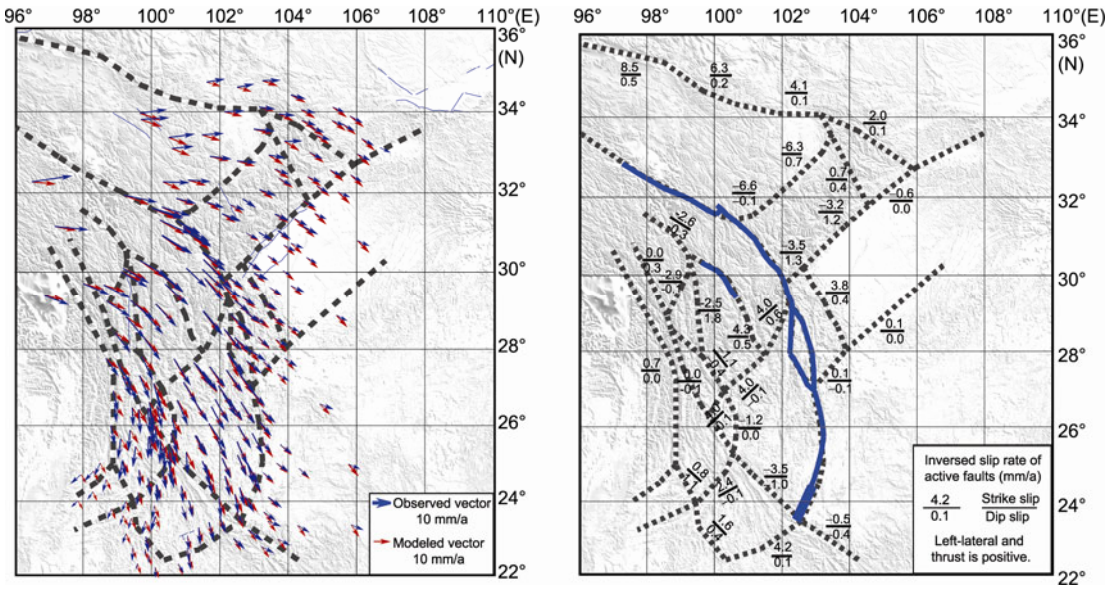

Figure 4 Inversion results of the slip rate in the Sichuan-Yunnan region.

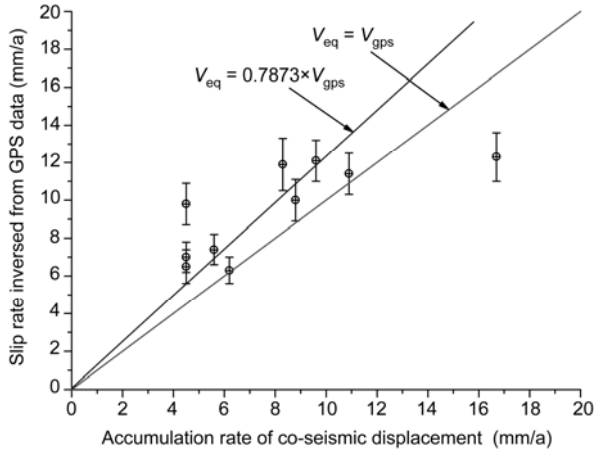

Figure 5 Comparison between V_{eq} and V_{gps}.

ruptured the whole segment even when the earthquake was not strong enough. In that case, the average co-seismic displacement $\bar{D}$ will be smaller. But the influence on other fault segments will change little, because the scalar moment is not changed. The parameters of these earthquakes are listed in Table 2.

The steps we used to calculate the potential displacement are as follows. First, we calculated the co-seismic deformation field caused by the earthquakes, then we inversed the adjustment of other segments in the co-seismic deformation field based on the geometric model of faults in the Sichuan-Yunnan region. This adjustment is just the influence on other faults in depth.

In order to calculate the co-seismic deformation field of earthquakes, the area was set to a network of 0.5°×0.5° grids with assumed GPS points on each grid point. In addition, we have also set an assumed GPS profile across each fault segment. Once an earthquake occurs, the co-seismic deformation field will be reflected on the GPS profile and other assumed GPS stations, which will reflect the potential adjustments of these fault segments.

In this paper these assumed GPS stations were used as a constraint to inverse the precise potential displacement in depth using the 3-D half-space elastic dislocation model [42].

First, we inversed the potential displacement of the seismogenic segment using the co-seismic displacement of all the assumed GPS stations. Then, we removed the GPS stations around the seismogenic segment from the network to inverse the potential displacement of the adjacent fault segments. Similarly, we removed the GPS stations around both the seismogenic fault segment and adjacent fault segments to inverse the potential displacement of the fault segments that are still farther away. Finally, we obtained the potential displacements of all the fault segments in the co-seismic deformation field. When we divide the potential displacement by V_{gps}, the Influence Value, which means by how many years the period of fault segment's earthquake energy accumulation will be lengthened or shortened, can be obtained. If we divide the Influence Value by CERP of the fault segment, we can get the Influence Degree of the fault segments.

Here the M_s8.0 earthquake on the GZ2 segment in 1854 can be taken as an example. First, we calculated the co-seismic deformation field of this earthquake using the 3-D half-space elastic dislocation model, in which the seismogenic layer ruptures abruptly while the dislocation layer is locked. Then we inversed the potential displacement in depth of the other fault segments. The results are shown in Figure 6.

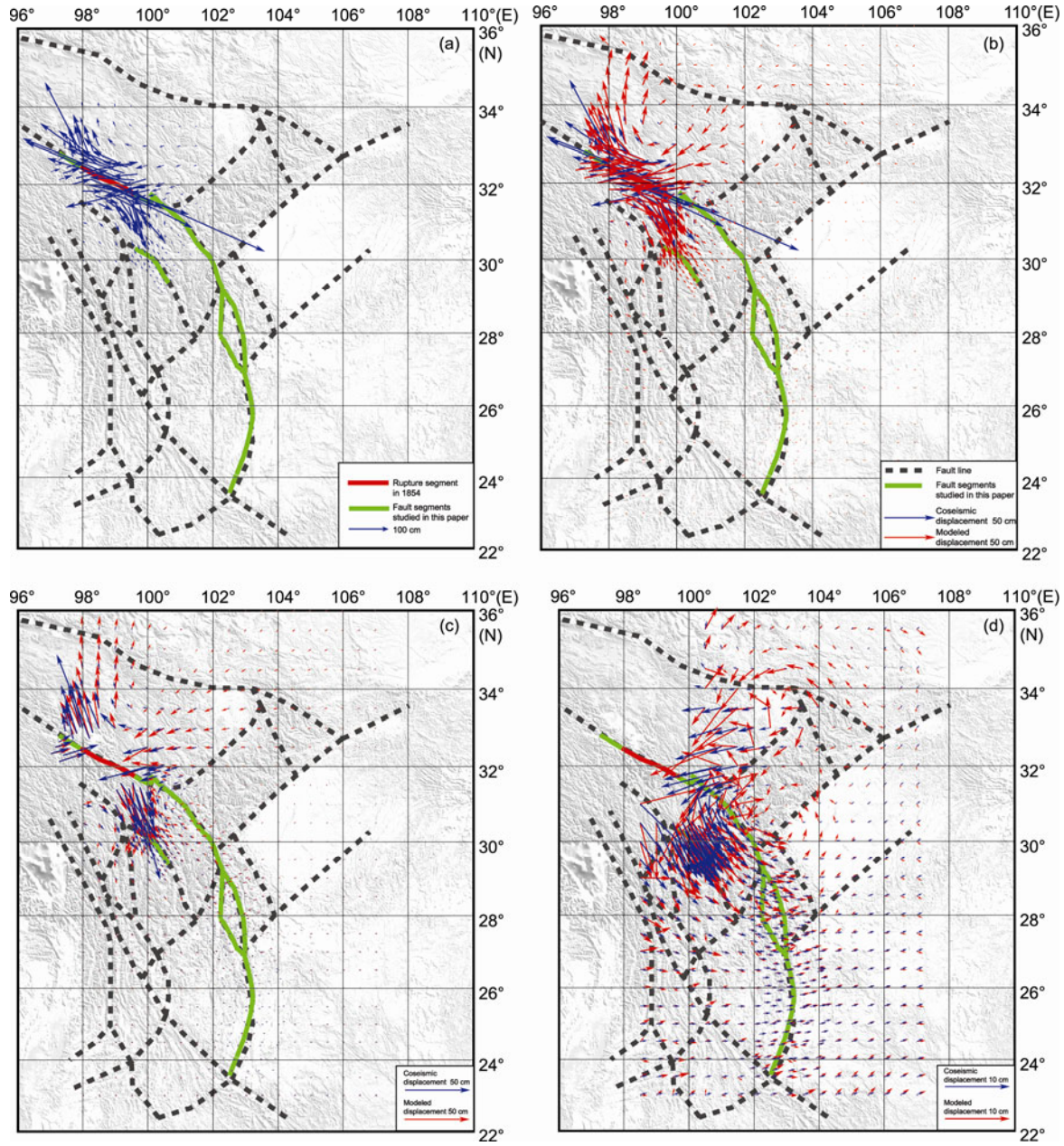

Figure 6 (a) Co-seismic deformation field of the earthquake in 1854; (b) inversion of the main rupture segment's potential displacement; (c) inversion of the adjacent segments' potential displacement; (d) inversion of the farther fault segments' potential displacement.

After the above calculations, we have got the influence of the earthquake in 1854 on other fault segments. If we divide this influence by V_{gps}, the Influence Value of the earthquake can be obtained. And the Influence Degree comes out when the Influence Value is divided by CERP. The results of Influence Degree are shown in Figure 7; positive stands for the increase of earthquake energy accumulation while negative the decrease of it.

From the results, we know that the influence values of the GZ1, GZ3 and GZIF segments are 29.3, 16.1 and 77.9 respectively in 1854, which make the energy accumulation of these fault segments increased. Also the influences are reflected on the segments of the Xianshuihe fault and the Litang fault, but not obvious on other segments. So we assumed that the earthquake in 1854 had moved up the occurrence time of characteristic earthquakes on GZ1 in 1896 and GZ3 in 1866. Similarly, other earthquakes also have some influences on these fault segments. Figure 7 gives our calculation results of all the influences.

3 Characteristics of strong earthquakes evolution

In order to get the Impending Earthquake Risk (hereafter we call it IER), which reflects the energy accumulation degree

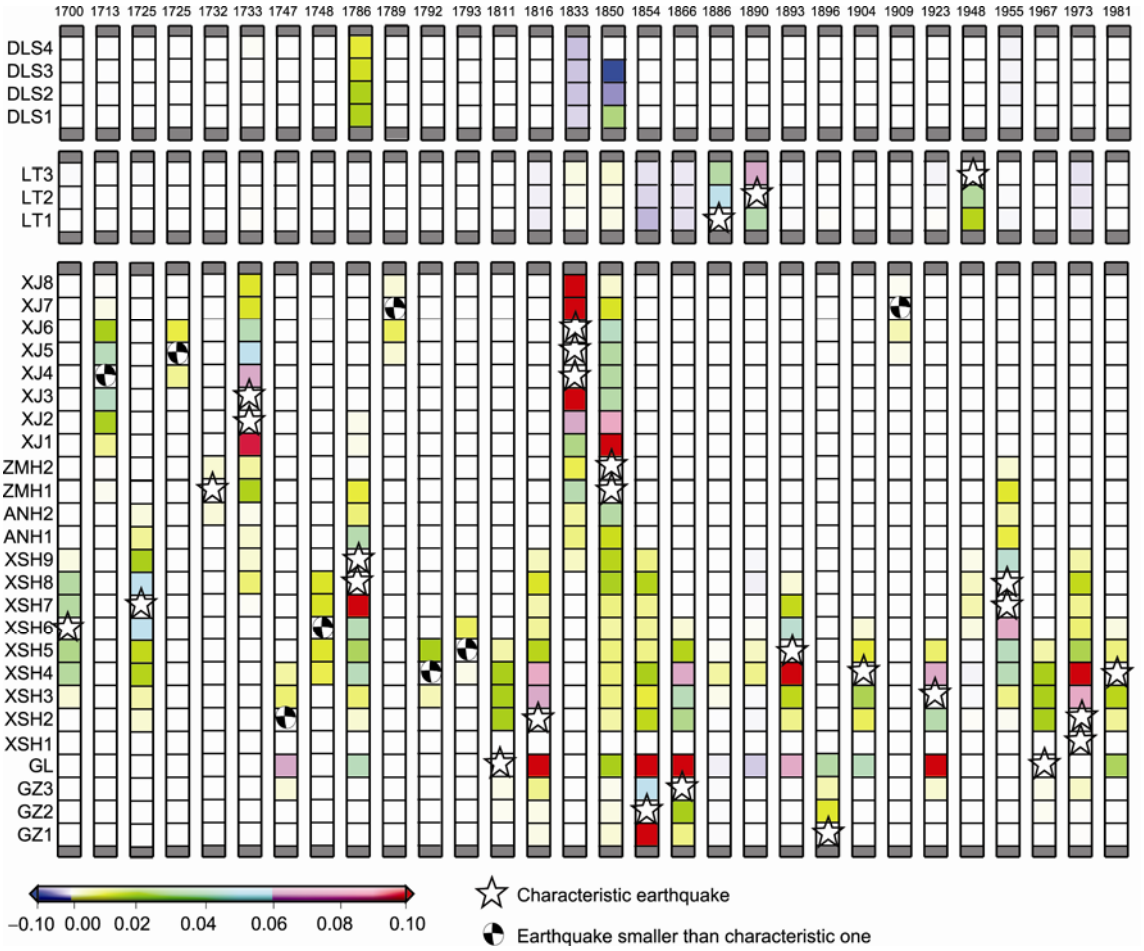

Figure 7 Map showing the interaction among earthquakes around the eastern boundary of Sichuan-Yunnan rhombic block. Abscissa shows the time of earthquake occurrence; ordinate shows fault segment hit by earthquake. Colored bar shows the influence value of the fault segments in each co-seismic deformation field, being –0.1 to 0.1 in most cases; the blue grid means that the influence value is negative; the white grid means negligible effects of the segments in co-seismic deformation field; other colored grid means that the influence value is positive.

and earthquake hazard risk of the fault segment, we studied the followings.

First, we divided the elapsed time by CERP to get the elapsed degree of the fault segment. In some cases, there may be earthquakes, which are not strong enough but have obvious energy release, to occur between two characteristic ones; we assumed them as having released some of the accumulated energy. So we deducted the average displacement caused by the earthquakes from the accumulated displacement at that time. The earthquake of XSH6 in 1748 is such an example; its magnitude is M_s6.8, smaller than the characteristic magnitude of M_s7.1.

Secondly, we added the influence degree into the elapsed degree to obtain the energy accumulation degree of each fault segment. The energy accumulation degree can be seen as the degree of earthquake risk and we call it Impending Earthquake Risk (IER). Figure 8 shows the IER of each fault segment just at the time before the earthquake occurred. The IER of historical earthquake cases can help us to see whether the earthquake risk can be known from IER.

As to the fault segment with no characteristic earthquake record, we thought the elapsed degree is 0 and the Impending Earthquake Risk (IER) could not be shown clearly but only can be assigned as 0.

We can see from the results that almost all the IER in history are larger than 1, i.e. 1.85 of the GL segment in 1967, 1.17 of the XSH4 segment in 1981, 1.31 of the XSH7 segment in 1955, 1.82 of the XSH8 segment in 1955, 4.92 of the XSH8 segment in 1786, and 1.62 of the XSH9 segment in 1786. Two exceptions are that the IER of ZMH1 segment in 1850 is 0.6 and the IER of XSH2 segment in 1973 is 0.75.

The most probable reasons that cause the IER on the large or small side may be as follows.

For the Luhuo earthquake that occurred in 1973 on the XSH1 and XSH2 segments, the IER of XSH2 segment is 0.75, smaller than 1. But we can see from Figure 3 and Table 2 that the V_{eq} calculated from the Recurrence Period of Characteristic Earthquake (CERP) is 12.3×0.7873 mm/a; it is much smaller than 16.7 mm/a, which is calculated from

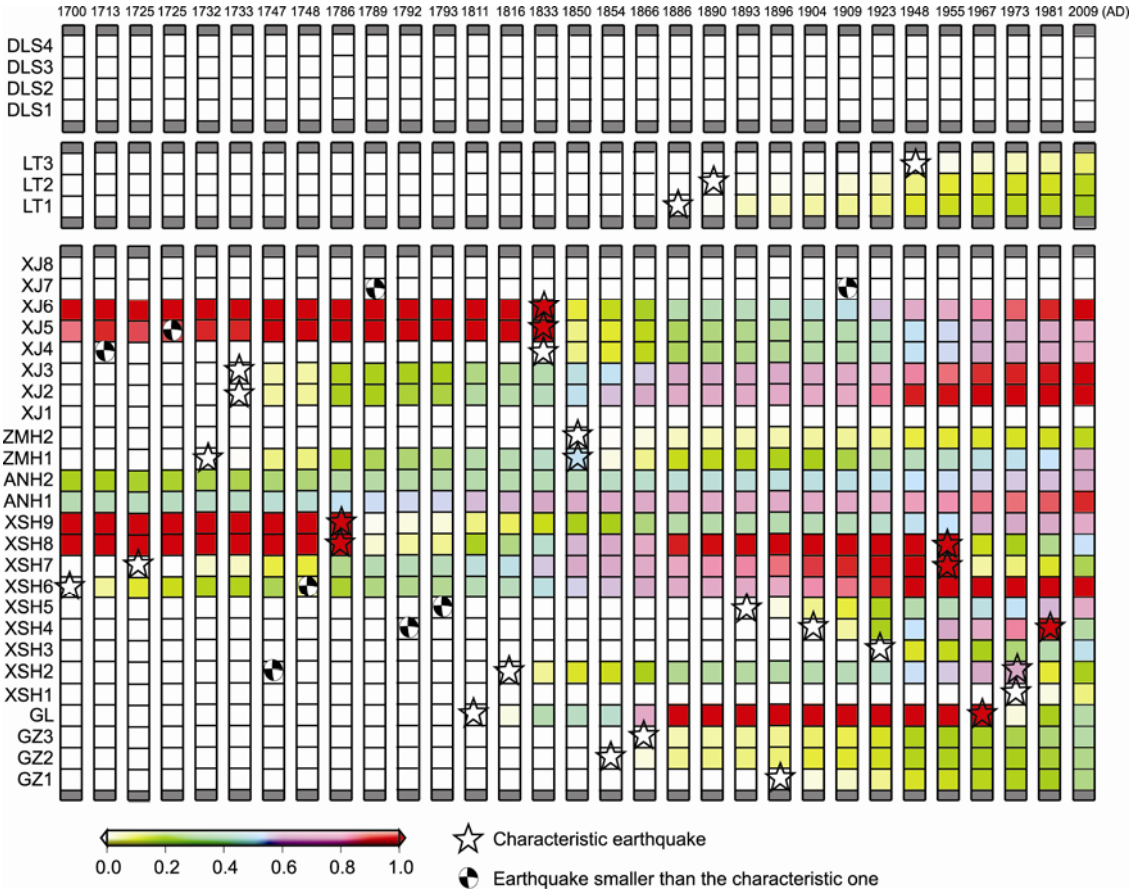

Figure 8 Impending Earthquake Risk around the east boundary faults of the Sichuan-Yunnan rhombic block. Abscissa shows the time of earthquake occurrence, ordinate shows fault segment hit by earthquake. Colored bars show the IER of fault segments in each co-seismic deformation field, different colors show different IER values of the fault segment, darkening color means increasing IER. When the IER is larger than 1, the fault segment is in danger of earthquake at any time; the IER is not clear when the grid color is white.

geological studies of historical earthquakes (Table 2). We thought that the smaller V_{eq} value may be due to the influence of XSH1 segment. The XSH1 segment, which lies at the tip of the Xianshuihe fault, was not ruptured in 1816 and enough energy may have accumulated for many years. The rupture of the XSH1 segment advanced the rupture of the XSH2 segment. So we got a smaller CERP and a larger V_{eq} (Figure 2 and Table 2). If we use 16.7 mm/a as V_{eq}, the IER will be 1.29, which may better represent IER of the XSH2 segment in 1973.

As to the XSH8 segment with IER of 4.92 larger than 1 in 1786, we thought this value cannot represent the real situation. The reasons are as follows. First, the length of XSH8 segment is small; and its rupture in 1955 may be caused by the influence from the XSH9 segment. Second, there may be earthquakes on the segment not recorded in history and the earthquake is not larger than M_s6.8, without surface rupture. And in 1850, the IER of ZMH1 is 0.6, smaller than 1. We assumed that the rupture of this segment might be induced by the rupture of the ZMH2 segment.

The IER of other fault segments can be considered as reasonable, because on each of these fault segments, at least two characteristic earthquakes have occurred in the time-window with reasonable recurrence time gap.

To sum up, the IER for the following fault segments are reasonable, 1.85 for the GL segment in 1967, 1.29 for the XSH2 segment in 1973, 1.17 for the XSH4 segment in 1981, 1.31 for the XSH7 segment in 1955, 1.82 for the XSH8 segment in 1955, and 1.62 for the XSH9 segment in 1786. It can be seen that all the IER above are close to or larger than 1.2 before historical earthquakes. Some reasons why the IER are close to or larger than 1.2 but not 1 are as follows. The CERP is not the real situation, but contains the influences from other earthquakes. In order to highlight the influences, we have calculated the influences again and added them into accumulated energy. Thus, the CERP we calculated is smaller, and the IER we calculated becomes higher.

In order to reflect both the interactions and the real situation, we did not use the elapsed time to judge the earthquake hazard risk but divided the IER by 1.17, which is the smallest one of the IER of the recurring earthquakes in history. The IER values of the recurring events are as follows: 1.58 for the GL segment in 1967, 1.10 for the XSH2 segment in 1973, 1 for the XSH4 segment in 1981, 1.12 for the XSH7

segment in 1955, 1.56 for the XSH8 segment in 1955, and 1.38 for the XSH9 segment in 1786. Until the year 2009, the IER values close to or larger than 1 corresponding to different fault segments are as follows, 1.35 for the Tagong segment of Xianshuihe fault (XSH6), 0.92 for the north segment of Anninghe fault (ANH1), 1.17 for the Menggu-Dongchuan segment of the Xiaojiang fault (XJ2), 1.04 for the Dongchuan-Xundian segment of the Xiaojiang fault (XJ3), and 1.09 for the Yiliang-Chengjiang segment of the Xiaojiang fault (XJ6). The results are consistent with the former studies from the maximum shear strain rate [43].

For some fault segments, including the Daliangshan fault (DLS1-DLS4), the Qiaojiang-Menggu segment of the Xiaojiang fault (XJ1), the Chengjiang-Tonghai segment of the Xiaojiang fault (XJ7), and the Tonghai-Jiangshui segment of the Xiaojiang fault (XJ8), we were unable to obtain the Impending Earthquake Risk (IER), but only calculated the influence degrees owing to the lack of the time when the latest earthquake occurred. The segment XSH1 is also a special case; it is located at the tip of the Xianshuihe fault, with unknown activity and fault length, so the influences from other earthquakes are not clear in this study.

4 Discussion and conclusions

The recurrence period of characteristic earthquakes, as the major evidence to judge the earthquake hazard risk, is a hot issue in earthquake studies. It is easy to obtain the Recurrence Period of Characteristic Earthquake (CERP) in the region with enough historical earthquake records and paleo-earthquake studies. But owing to the difficulty of paleo-earthquake research and short period of historical earthquake records, it is difficult to obtain the CERP of all the segments.

Fortunately, the application of GPS on crustal deformation gives us an opportunity to know the present-day slip rate of the active faults and makes the precise studies on the assessment of earthquake risk possible. Taking the two aspects above into consideration, we can obtain V_{eq} and V_{gps} from geological survey and GPS studies in some fault segments at first, and then get a characteristic relationship between them at these segments. After that, by using this relation and all the V_{gps} inversed from GPS, we can get all V_{eq}. We have got the statistic relationship between V_{gps} and V_{eq} in eq. (9), which means V_{eq} is always less than V_{gps}, V_{gps} can be seen as the slip rate of the fault segment in the geological history, and V_{eq} is considered equal to V_{gps} less V_c, and V_c is the creep rate [44].

Finally we can divide the average co-seismic displacement by V_{eq}, and all the CERP will be obtained. Based on the rupture parameters we calculated, we have studied the interrelation of historical earthquakes and strong earthquakes evolution.

After the above studies, we conclude, Owing to the interaction among earthquakes and fault segments, once an earthquake occurs on a segment of the east boundary fault zone of the Chuan-Yunnan rhombic block, especially a large event, it will influence the surrounding fault segments more or less; the influence degree on other fault segments depends not only on the earthquake's magnitude but also on the present slip rate (V_{gps}) and geometric scale of those segments.

Because the Xianshuihe fault, the Anninghe fault, the Zemuhe fault, and the Xiaojiang fault have the common characters of left-lateral strike slip, the influences on their segments from the earthquakes occurring on these faults are always promoting the energy accumulation. The Litang fault, which is parallel to the Xianshuihe fault, accepts both positive and negative influences from earthquakes on other segments in increasing the energy accumulation. As to the Daliangshan fault, the influence values on this fault are not always positive; in particular, the M_s8.0 earthquake occurring on the Zemuhe fault has great influence on it, and the influence on the Tuodu-Butuo segment (DLS3) is the most obvious in mitigating the energy accumulation.

As to the results of IER, we can find that the IER of the previous earthquakes are always larger than 1 (Figure 8). At present, there are four segments with IER larger than 1, i.e. the Tagong segment of the Xianshuihe fault, the Menggu-Dongchuan segment of the Xiaojiang fault, the Dongchuan-Xundian segment of the Xiaojiang fault, and the Yiliang-Chengjiang segment of the Xiaojiang fault, for which the IRE values are 1.35, 1.17, 1.04 and 1.09, respectively. So these segments might be in a dangerous state. Also attention should be paid to the north segment of the Anninghe fault with IER of 0.92.

This work was supported by the National Basic Research Program of China (Grant No. 2008CB425704) and the Open Foundation of State Key Laboratory of Earthquake Dynamics (Grant No. LED2009B02). We are grateful to Professor Wen Xueze for his specific data of fault segments and discussion on the historical earthquake research. The figures were drawn using the GMT tools.

1 Kan R J, Zhang S C, Yan F T, et al. Present tectonic stress field and its relation to the characteristics of recent tectonic activity in southwestern China (in Chinese). Acta Geophys Sin, 1977, 20: 96–109
2 Wen X Z. Rupture segmentation and assessment of probabilities of seismic potential on the Xiaojiang fault zone (in Chinese). Acta Seismol Sin, 1993, 6: 993–1004
3 Li P. Xianshuihe-Xiaojiang Fault Zone (in Chinese). Beijing: Seismological Press, 1993. 7–28
4 Allen C R, Han Y, Sieh K E, et al. Red River and associated faults, Yunnan Province, China, Quaternary geology, slip rates, and seismic harzard. Geol Soc Am Bull, 1984, 95: 686–700
5 Xu X W, Zhang P Z, Wen X Z, et al. Features of active tectonics and recurrence behaviors of strong earthquakes in western Sichuan Province and its adjacent regions (in Chinese). Seismol Geol, 2005, 27: 446–461
6 Wang Y Z, Wang E N, Shen Z K, et al. GPS-constrained inversion of present-day slip rates along major faults of the Sichuan-Yunnan region, China. Sci China Ser D-Earth Sci, 2008, 51: 1267–1283
7 Shen Z K, Lu J N, Wang M, et al. Contemporary crustal deformation

around the southeast borderland of the Tibetan Plateau. J Geophys Res, 2005, 110: B11409
8 Wen X Z, Ma S L, Xu X W. Historical pattern and behavior of earthquake ruptures along the eastern boundary of the Sichuan-Yunnan faulted-block, southwestern China. Phys Earth Planet Inter, 2008, 168: 16–36
9 Xu X W, Wen X Z, Yu G H, et al. Average slip rate, earthquake rupturing segmentation and recurrence behavior on the Litang fault zone, western Sichuan Province. Sci China Ser D-Earth Sci, 2005, 48: 1183–1196
10 Song F M, Li R C, Xu X W. Preliminary results of the investigation of paleo-earthquakes along the Daliangshan fault zone, Sichuan Province, China (in Chinese). Seismol Geol, 2002, 24: 27–34
11 He H L, Yasuta I, He Y L, et al. Newly-generated Daliangshan fault zone-shortcutting on the central section of Xianshuihe-Xiaojiang fault system. Sci China Ser D-Earth Sci, 2008, 51: 1248–1258
12 Ren J W. Preliminary study of the recurrence period of strong earthquakes on the fracture zone of Zemuhe, west Sichuan (in Chinese). Inland Earthq, 1990, 4: 107–115
13 Ran Y K, Chen L C, Chen J W, et al. Late quaternary surface deformation and rupture behavior of strong earthquake on the segment north of Mianning of the Anninghe fault. Sci China Ser D-Earth Sci, 2008, 51: 1224–1237
14 Zhang Q W, Zhang P Z, Wang C, et al. Interaction of active faults and its effect on earthquake triggering and delaying (in Chinese). Acta Geosci Sin, 2004, 25: 483–488
15 Wang H, Liu J, Shi Y L, et al. Dynamic simulation of interactions between major earthquakes on the Xianshuihe fault zone. Sci China Ser D-Earth Sci, 2008, 51: 1388–1400
16 Papadimitriou E E, Wen X Z, Karakostas V G, et al. Earthquake triggering along the Xianshuihe fault zone of western Sichuan, China. Pure Appl Geophys, 2004, 161: 1683–1707
17 Slemmons D B. A procedure for analyzing fault-controlled lineament and active fault. In: Proceedings 3rd International Conference on Basement Tectonic Association, 1982. 33
18 Wen X Z. Character of rupture segmentation of the Xianshuihe-Anninghe-Zemuhe fault zone, Western Sichuan (in Chinese). Seismol Geol, 2000, 22: 239–249
19 Zhang C L, Ren J W. Recent movement pattern along the Zemuhe fault and deformation indicators for its identification (in Chinese). Seismol Geol, 1995, 17: 427–431
20 Huang S M. Preliminary study of features of strong historic earthquaks and the assessment information of the general seismic trend (in Chinese). J Seismol Res, 1985, 8: 485–495
21 Wen X Z, Ma S L, Lei X N, et al. Newly found surface rupture remains of large historical earthquakes on and near transition segment of the Anninghe and Zemuhe fault zones, Western Sichuan, China (in Chinese). Seismol Geol, 2007, 29: 826–833
22 Wen X Z, Xu X W, Zheng R Z, et al. Average slip-rate and recent large earthquake ruptures along the Garzê-Yushu fault. Sci China Ser D-Earth Sci, 2003, 46(Suppl): 276–288
23 Pei X Y, Wang X M, Zhang C G. Basic segmentation characteristics on late quarternary Anninghe active faults (in Chinese). Earthq Res Sichuan, 1998, (4): 52–61
24 Xu X W, Wen X Z, Zheng R Z, et al. Pattern of latest tectonic motion and its dynamics for active blocks in Sichuan-Yunnan region, China. Sci China Ser D-Earth Sci, 2003, 46(Suppl 1): 210–226
25 Tang R C, Han W B. Active Faults and Earthquakes in Sichuan Province, China (in Chinese). Beijing: Seismological Press, 1993. 149–152
26 Wen X Z. Conditional probabilities for the recurrence of earthquakes on the Xianshuihe fault zone within the coming three decades (in Chinese). Earthq Res Chin, 1990, 6: 8–16
27 Zhou R J, He Y L, Huang Z Z. The slip part and strong earthquake recurrence interval on the Qianning-Kangding segment of the Xianshuihe fault zone (in Chinese). Acta Seismol Sin, 2001, 23: 250–261
28 Yu W X, Liu Y Q, He W. Characters of recent crustal deformation and earthquakes on the Xiaojiang fault zone in Yunnan Province (in Chinese). Seismol Geol, 1997, (1): 17–21
29 Guo Z, Qin B. Physics of Seismic Sources (in Chinese). Beijing: Seismological Press, 1979. 35–103
30 Deng Q, Yu G H, Ye W H. Relationship between earthquake magnitude and parameters of surface ruptures associated with historical earthquakes (in Chinese). In: Institute of Geology, SSB, ed. Research on Active Fault (2). Beijing: Seismological Press, 1991. 247–264
31 Wells D L, Coppersmith. New empirical relationships among magnitude, rupture length, rupture width, rupture area, and surface displacement. Bull Geol Soc Am, 1994, 84: 974–1002
32 Zhong Y Y, Zhu X Y, Zhang Z F. Study on relations between seismic moment and magnitude for various types of earthquake sequence (in Chinese). Northwestern Seismol J, 2004, 26: 57–61
33 Heim A. Earthquake region of Taofu. Bull Geol Soc Am, 1934, 45: 1035–1050
34 Wen X Z. Segmentation, geometric features, and their seimotectonic implications for the Holocene Xianshuihe fault zone (in Chinese). Acta Seismol Sin, 1989, 11: 360–370
35 Zhu A L, Xu X W, Zhou Y S, et al. Relocation of small earthquakes in western Sichuan, China and its implications for active tectonics. Chin J Geophys, 2005, 48: 629–636
36 Okada Y. Surface deformation due to shear and tensile faults in a half-space. Bull Seism Soc Am, 1985, 75: 1135–1154
37 Okada Y. Internal deformation due to shear and tensile faults in a half-space. Bull Seism Soc Am, 1992, 82: 1018–1040
38 Savage J C , Svarc J L, Prescott W H. Geodetic estimates of fault slip rates in the San Francisco Bay area. J Geophys Res, 1999, 104: 4995–5002
39 Gan W, Svarc J L, Savage J C, et al. Strain accumulation across the Eastern California Shear Zone at latitude 36°30′N. J Geophys Res, 2000, 105: 16229–16236
40 Cheng J, Gan W, Wang Z, et al. The simulation of background crustal deformation field of the M_S8.1 Kunlun earthquake of 2001 (in Chinese). Seismol Geol, 2009, 31: 97–111
41 Gan W J, Zhang P Z, Shen Z K, et al. Present-day crustal motion within the Tibetan Plateau inferred from GPS measurements. J Geophys Res, 2007, 112: B08416
42 Cheng J, Liu J, Gan W, et al. The influence of 2008 Wenchuan earthquake on earthquake occurrence trend of active faults in Sichuan-Yunnan region. Earthq Sci, 2009, 22: 459–470
43 Shen Z K, Wang M, Gan W, et al. Contemporary tectonic strain rate field of Chinese continent and its geodynamic implications (in Chinese). Earthq Sci Front, 2003, 10(Suppl): 93–100
44 Wallace R E. Earthquake intervals on the San Andreas fault. Geol Soc Am Bull, 1970, 88: 1276